Complex EOF Analysis as a Method to Separate Barotropic and Baroclinic Velocity Structure in Shallow Water

CATHERINE R. EDWARDS AND HARVEY E. SEIM

Department of Marine Sciences, University of North Carolina at Chapel Hill, Chapel Hill, North Carolina

(Manuscript received 9 March 2007, in final form 13 September 2007)

ABSTRACT

Defining the vertical depth average of measured currents to be barotropic is a widely used method of separating barotropic and baroclinic tidal currents in the ocean. Away from the surface and bottom boundary layers, depth-averaging measured velocity is an excellent estimate of barotropic tidal flow, and internal tidal dynamics can be well represented by the difference between the measured currents and their depth average in the vertical. However, in shallow and/or energetic tidal environments such as the shelf of the South Atlantic Bight (SAB), bottom boundary layers can occupy a significant fraction of the water column, and depth averaging through the bottom boundary layer can overestimate the barotropic current by several tens of centimeters per second near bottom. The depth-averaged current fails to capture the bottom boundary layer structure associated with the barotropic tidal signal, and the resultant estimate of baroclinic tidal currents can mimic a bottom-trapped internal tide.

Complex empirical orthogonal function (CEOF) analysis is proposed as a method to retain frictional effects in the estimate of the barotropic tidal currents and allow an improved determination of the baroclinic currents. The method is applied to a midshelf region of the SAB dominated by tides and friction to quantify the effectiveness of CEOF analysis to represent internal structure underlying a strong barotropic signal in shallow water. Using examples of synthesized and measured data, EOF estimates of the barotropic and baroclinic modes of motion are compared to those made using depth averaging. The estimates of barotropic tidal motion using depth-averaging and CEOF methods produce conflicting predictions of the frequencies at which there is meaningful baroclinic variability. The CEOF method preserves the frictional boundary layer as part of the barotropic tidal current structure in the gravest mode, providing a more accurate representation of internal structure in higher modes. The application of CEOF techniques to isolate internal structure co-occurring with highly energetic tidal dynamics in shallow water is a significant test of the method. Successful separation of barotropic and baroclinic modes of motion suggests that, by fully capturing the effects of friction associated with the barotropic tide, CEOF analysis is a viable technique to facilitate examination of the internal tide in similar environments.

1. Introduction

Internal tides have been widely studied over the coastal ocean and can be important pathways of energy transfer from the barotropic tide to dissipation and mixing in shallow water (e.g., Huthnance 1989; MacKinnon and Gregg 2003b; Rippeth and Inall 2002; Holloway et al. 2001). However, separating the baroclinic tidal motion from the barotropic currents in measured data can be a challenge because of both barotropic and baroclinic motions operating at the same frequency, but with different vertical and temporal modes of variability. The traditional approach has been to assume that baroclinic motions are responsible for observed vertical shear at tidal frequencies and assign the barotropic currents to be the depth average of measured data. However, in shallow water, development of boundary layers near the surface or bottom can add significant shear to the barotropic tidal current profile. A standard time series analysis technique is investigated to determine if it can isolate internal modes of motion in shallow regions where bottom boundary layers can occupy a significant fraction of the water column.

Complex empirical orthogonal function (CEOF) analysis is proposed as a better alternative to depth-averaging methods to estimate barotropic tidal currents from measured data, allowing an improved representa-

Corresponding author address: Catherine Edwards, Department of Marine Sciences, University of North Carolina at Chapel Hill, 340 Chapman Hall, CB #3300, Chapel Hill, NC 27599.
E-mail: catherine.edwards@unc.edu

DOI: 10.1175/2007JTECHO562.1

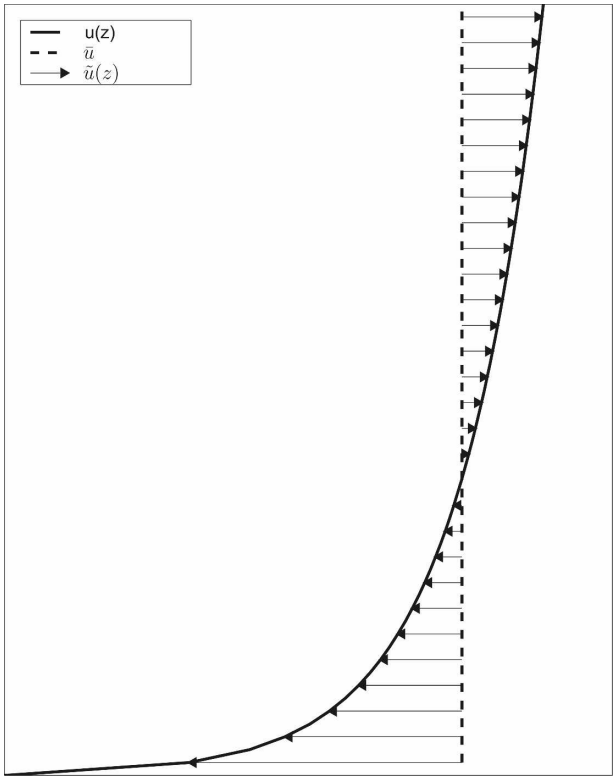

FIG. 1. Cartoon showing the potential effect of depth averaging a barotropic flow through a strong bottom boundary layer in shallow water. The thick line denotes $u(z)$, the depth average of which is $\bar{u}$, represented as the dashed line. The arrows show the magnitude and direction of $\tilde{u}(z) \equiv u(z) - \bar{u}$.

tion of internal tidal motions. Away from the surface and bottom boundary layers, depth-averaging measured velocity can give an excellent estimate of barotropic tidal flow, and is a widely used method for separating barotropic and baroclinic tidal currents in the coastal ocean. Depth averaging can provide reasonable estimates of a relatively weak barotropic tidal current in moderately shallow water (e.g., MacKinnon and Gregg 2003a), of a stronger barotropic tide in deeper water (e.g., Holloway et al. 2001; Rippeth and Inall 2002), or of relatively weak tides over a range of depths (e.g., Lerczak et al. 2003).

Where the bottom boundary layer occupies a significant fraction of the water column, depth averaging a current profile $u(z, t)$ and subtracting the depth average $\bar{u}_z(t)$ from every point in the profile to remove the barotropic current can leave a boundary layer signature in the difference. Figure 1 depicts a cartoon snapshot of an idealized one-dimensional barotropic tidal current profile in shallow water $u(z)$, its depth average $\bar{u}$, and $\tilde{u}(z) \equiv u(z) - \bar{u}$. When $u(z)$ is an oscillating current, the difference $\tilde{u}(z)$ has a 180° temporal phase difference surface to bottom and can resemble an internal tide trapped near bottom, where the bottom boundary layer effects are greatest. Simionato et al. (2005) define the baroclinic velocity by subtracting the depth average of measured current profiles in the Rio de Plata Estuary, Brazil, and report a slightly bottom-enhanced M_2 internal tide near the mouth of the estuary. Though the Rio de Plata is classified as a microtidal system, the use of depth averaging in 15 m of water suggests that the bottom boundary layer structure principally associated with the barotropic tidal dynamics may have been mistakenly identified to result from an internal tide.

Complex EOF analysis is investigated herein as a tool that can account for the bottom boundary layer structure of barotropic tidal currents, allowing a better isolation of the current structure of internal tides and waves in the vertical. Several studies have employed similar analyses to describe the vertical structure of shallow water currents. However, the input time series are typically low-pass filtered to examine subtidal dynamics (Webster 1986; Münchow and Chant 2000), harmonically analyzed to remove the tide (Lentz 1994), and analyzed as the difference between model solutions with tidal and/or wind forcing (Hall and Davies 2002) or those in which the barotropic tide at that frequency could be neglected altogether (Lerczak et al. 2003). Apel et al. (1997) use real-valued EOF analysis to identify the vertical structure of currents measured on the outer shelf of the Mid-Atlantic Bight (MAB), but the tidal environment and ADCP configuration were such that the barotropic currents had no appreciable vertical structure. Thus, while the use of EOF and CEOF analyses to examine internal structure is reflected in the literature, the application of the method to unfiltered currents in a highly energetic shallow water environment has not been reported. Successful isolation of internal tidal structure in such an environment is an important test of the method.

Flows on the midshelf of the South Atlantic Bight (SAB) are largely controlled by the tides and the wind (Lee et al. 1991). It is estimated that 80%–90% of cross-shelf and 20%–40% of alongshelf current variance can be attributed to the tidal band (Tebeau and Lee 1979; Lee and Brooks 1979). The M_2 tide, significantly amplified over the shelf (Redfield 1958) and with current ellipses oriented cross-shore, accounts for much of this variance, with current magnitudes on the order of 30–40 cm s^{-1} (Blanton et al. 2004). The shallow depth of the SAB (typically less than 50 m) and the magnitude of the M_2 tide found on the shelf result in significant frictional shear over much of the water column. The combined effect of strong tidal currents and the associated bottom boundary layer structure that develops in the

SAB can significantly hinder clean separation of the barotropic and baroclinic velocity structures. As can be seen in Fig. 1, the depth-averaged current fails to capture the free-stream velocity and leads to a small underestimate of the barotropic current near surface that can be several centimeters per second. The effect is most acute at the base of the water column; an overestimate of the barotropic current by $\overline{u}_z(t)$ near bottom could potentially be tens of centimeters per second. Depth averaging through veering within the tidal bottom boundary layer further confounds the separation of barotropic and baroclinic velocity structures by introducing errors in estimates of barotropic tidal phase and orientation.

To quantify the ability of EOF analysis to isolate a barotropic signal in shallow water, the EOF method is applied to midshelf tidal currents synthesized using a purely barotropic formulation of vertical structure, and the results are compared to those using depth-averaging methods. The analysis is repeated for measured current data acquired in a midshelf location in the SAB. Interpretation of the analysis and potential sources of error are presented, and practical considerations of the methods are discussed.

2. Methods

The CEOF technique (e.g., Davis 1976; Horel 1984; Barnett 1985; Preisendorfer 1988; Kaihatu et al. 1998) serves as a separation of variables in space and time. Here it is applied to the complex time series $\psi(z, t) = u(z, t) + i\upsilon(z, t)$, where u and υ are the eastward and northward positive components of velocity and $i = \sqrt{-1}$. The eigenvalue problem is solved for the complex covariance matrix formed from the time-varying portion of $\psi(z, t)$; the eigenvectors $\phi_j(z)$ describe independent vertical modes, and the eigenvalues λ_j give the variance associated with each mode. Temporal variability of the jth vertical mode at depth level m, ϕ_{jm}, is given by the projection of the data onto that mode:

$$a_j(t) = \sum_{m=0}^{M-1} \psi_m(t)\phi_{jm}, \tag{1}$$

where m is the modal index, less than or equal to the number of vertical levels M. Time series of the jth mode profile $\hat{\psi}_j$ can be reconstructed simply as a spatial time series:

$$\hat{\psi}_j(z, t) = a_j(t)\phi_j^*(z), \tag{2}$$

where the asterisk (*) denotes the complex conjugate.

Kaihatu et al. (1998) argue that this CEOF formulation converges faster than real-valued EOF analysis by component, but loses some meaning of the vector projection, citing Preisendorfer's (1988) caution that directionality can become ambiguous in the eigenvalue search. In this application to the SAB, the principal axes of the flow are well-defined, and representation of the rotary tidal currents does not require independence of the along- and cross-shore components of flow. That the CEOF coefficients are complex yields a more intuitive physical interpretation than the two-dimensional spatial problem; the vertical profile of a given mode retains its shape, but dilates and contracts in the horizontal as it rotates over a tidal cycle. Similarly, the limitation that the CEOF method can only represent two dimensions simultaneously is not a concern for this application.

For this application to the SAB, the barotropic tide is dominant and has been shown to contain the bulk of the variance of the currents. It is then assumed that the lowest vertical mode $\hat{\psi}_0(z, t)$ captures the structure of the barotropic tide and of other motions associated with free surface tilt and friction. The sum of the higher modes $\hat{\psi}_j(z, t)$ from $j = 1$ to $J = M - 1$ are interpreted to represent baroclinic motions.

3. Application to synthetic and measured current profiles

Part of the South Atlantic Bight Synoptic Offshore Observational Network (SABSOON; Seim 2000) network of real-time observational towers in the SAB, the R_6 tower is located near the 32-m isobath approximately 60 km offshore of Savannah, Georgia (Fig. 2). The combined effects of strong tides, wind stress, and shallow depth yield a frictionally dominant system, where the surface and bottom frictional boundary layers can potentially merge.

To estimate the barotropic and internal tidal structure, CEOF and depth-averaging methods are applied to synthetic and measured time series of current profiles at R_6. Synthetic tidal current profiles for this midshelf location are constructed using a purely barotropic formulation (described below) resulting in a known vertical structure and internal tidal currents of zero magnitude. Measured ADCP data from the month of October 2002 are chosen as a second case study for comparison of the performance of depth-averaging and CEOF estimates of barotropic and baroclinic tidal currents. The observations were acquired under well-mixed conditions, which minimizes the internal structure in the measured currents. Monthly averaged winds at R_6 were weakly downwelling-favorable toward the southwest, characteristic of autumn, and cross-shore monthly mean currents suggest little cross-shelf exchange. Collocated wind measurements over October

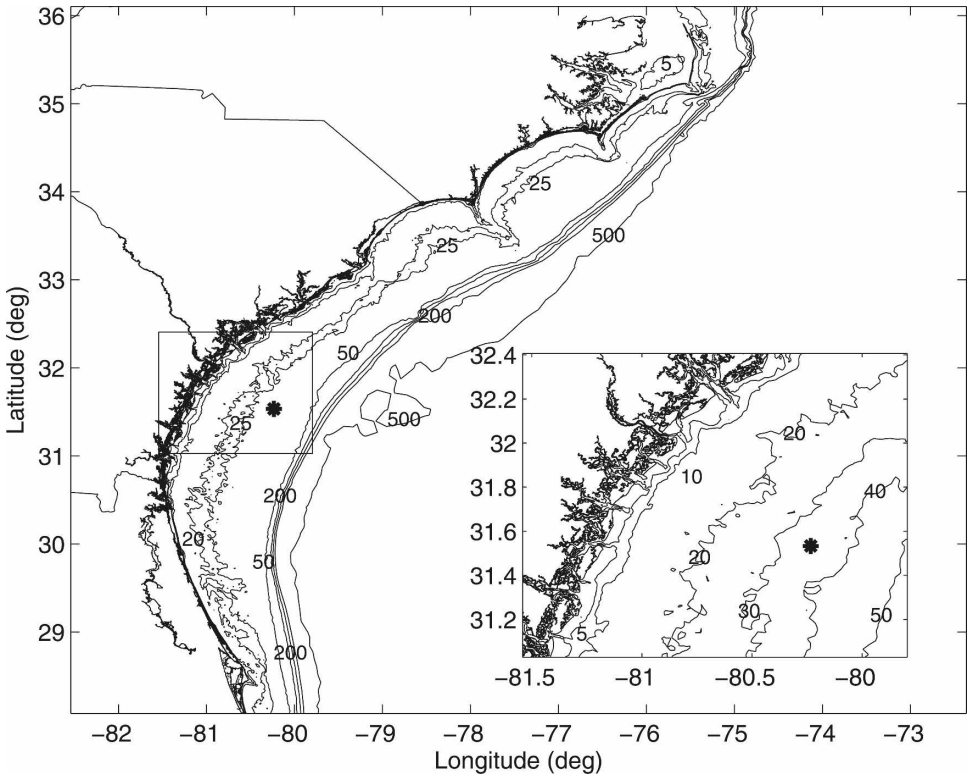

FIG. 2. Bottom topography of the SAB, with location of the R_6 tower indicated by the asterisk.

2002 reflect the passage of synoptic-scale atmospheric storms through the region every 5–8 days, yielding a well-mixed midshelf region with slight surface cooling, consistent with typical autumn conditions (Weber and Blanton 1980).

The barotropic tide is the dominant signal in the observations and precise estimates of bottom boundary layer structure are necessary to examine any potential internal tide, as $\tilde{u}(z)$ can be on the order of several to tens of centimeters per second, with a vertical structure that could easily be mistaken as arising from a baroclinic process. Barotropic tidal dynamics are relatively well understood in the SAB, and the discrete frequencies at which the tides occur allow a clear interpretation of the successes and failures of each method in removing the barotropic signal. For these reasons, tidal analysis is used to compare the CEOF and depth-averaged estimates of the barotropic tide for synthetic and ADCP-measured currents.

a. Synthetic tidal data

Idealized profiles of tidal currents at the R_6 tower are chosen as a simple representation of barotropic flow at the midshelf location. Amplitudes and phases of the depth-averaged M_2 tide are calculated using the South Atlantic Bight tidal database derived from the shelf-wide observational and modeling study of Blanton et al. (2004). A reasonable vertical structure is then computed using the analytical solution to a linear eddy viscosity model given and described by Soulsby (1990), using frictional parameters derived from a fit to tidal currents measured above the log layer. The roughness length z_0 was chosen to be 0.06 m based on observational estimates of 0.02–0.10 m derived from independent ADCP measurements and a linear one-dimensional turbulence closure model (M. Muglia 2003, personal communication). Using this value of z_0 and eddy viscosity profiles estimated under unstratified autumn conditions, $\hat{u}_*$ was chosen to be 0.099 m s^{-1}. The free-stream boundary condition to the solution is adjusted such that the integral over the resulting profile from the z_0 to the surface matches the depth-averaged current in the database. Time series over the month of October 2002 were then constructed from the resulting vertical profiles, with 1-h temporal resolution and 1-m increments from 3.5 to 27.5 m above the bottom (mab), matching those of the ADCP records analyzed in the following section.

The resulting synthetic time series of vertical profiles of the M_2 tidal currents are then decomposed into empirical vertical modes through CEOF analysis. The

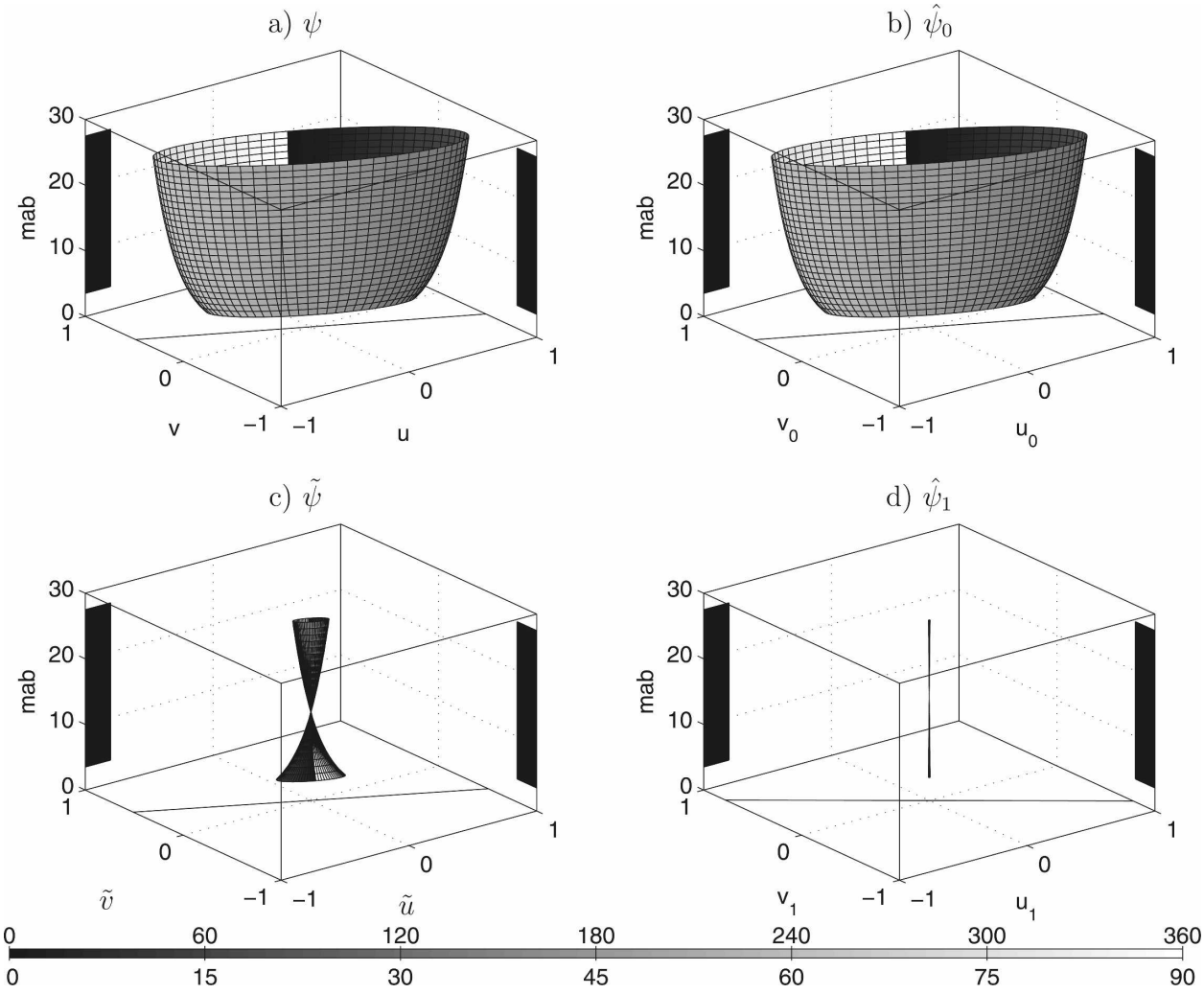

FIG. 3. Normalized M_2 tidal ellipses and 95% CIs about calculated ellipse parameters for synthetic M_2 input: (a) the original signal $\psi(z, t)$, (b) $\hat{\psi}_0(z, t)$, (c) $\tilde{\psi}(z, t)$, and (d) $\hat{\psi}_1(z, t)$. Ellipse phase is contoured along the ellipse on the upper color scale. Near-surface ellipse orientation is shown as a thin line for reference; vertically averaged semimajor and semiminor axis CIs about the near-surface ellipse are shown as thick lines, and orientation and phase CIs are contoured on the left and right corners of the plot, respectively, using the lower color scale. Ellipse semiaxes and CIs are normalized by the semimajor axis of the near-surface ellipse of the original signal shown in (a). All ellipses are plotted on the same scale for emphasis.

CEOF analysis is expected to recover the full signal $\psi(z, t)$ in its gravest mode, as its temporal variability is independent of its shape in the vertical; energy in higher modes indicates error in the analysis. Time series of each reconstructed mode $\hat{\psi}_j(z, t)$ are fit to the astronomical tide at each depth level using the least squares analysis of Pawlowicz et al. (2002). Defining $\overline{\psi}_z(t)$ to be the vertical depth average of $\psi(z, t)$ and $\tilde{\psi}(z, t) \equiv \psi(z, t) - \overline{\psi}_z(t)$ to be the complex number analog of $\tilde{u}(z, t)$ shown in Fig. 1, tidal analysis is repeated for the estimates of barotropic and baroclinic current structure using depth-averaging methods. Tidal ellipses of $\psi(z, t)$, $\hat{\psi}_j(z, t)$, and $\tilde{\psi}(z, t)$ are then compared at each depth level. For brevity, the (z, t) dependence is omitted in the description below but is implied unless otherwise specified.

The tidal ellipses and the 95% confidence intervals (CIs) about the ellipse parameter estimates derived from the least squares fit to the original signal ψ, $\tilde{\psi}$ are examined (Fig. 3), and the first two EOF modes $\hat{\psi}_0$ and $\hat{\psi}_1$. All tidal ellipses are normalized with respect to the semimajor axis of the near-surface synthetic ellipse. The lowest mode, $\hat{\psi}_0$, contains more than 99.998% of the variance of the input signal; $\hat{\psi}_1$ represents 0.001% of the variance, and is the only other mode with computable variance. Both $\hat{\psi}_1$ and $\tilde{\psi}$ show a 180° phase difference between the upper and lower layer, but the $\tilde{\psi}$ ellipses (Fig. 3c) are two orders of magnitude larger

TABLE 1. (left) Synthetic near-surface tidal ellipse parameters for the five largest tidal constituents for the specified input signal $\psi(z, t)$, and the depth-average of the (top right) 30-day synthesized current $\overline{\psi}_z(t)$ and (bottom right) lowest CEOF mode $\hat{\psi}_0(z, t)$. The 95% CI about the ellipse parameter estimates for $\overline{\psi}_z(t)$ and for $\hat{\psi}_0(z, t)$ are given.

Tidal constituent	u_{major} (cm s^{-1}) ψ	ψ_z $\hat{\psi}$	u_{minor} (cm s^{-1}) ψ	ψ_z $\hat{\psi}$	Inclination (deg) ψ	ψ_z $\hat{\psi}$	Phase (deg) ψ	ψ_z $\hat{\psi}$
M_2	38.15	33.77 ± 3.60	−13.31	−11.74 ± 1.28	153.87	154.01 ± 0.10	280.48	280.16 ± 0.24
		38.16 ± 7.3e-05		−13.27 ± 2.1e-04		154.06 ± 0.15		280.18 ± 0.24
N_2	8.30	7.35 ± 0.78	−2.88	−2.54 ± 0.28	152.34	152.48 ± 0.10	264.54	264.22 ± 0.23
		8.31 ± 1.4e-05		−2.87 ± 4.7e-05		152.52 ± 0.15		264.24 ± 0.23
S_2	4.34	3.84 ± 0.41	−1.43	−1.26 ± 0.14	152.22	152.36 ± 0.10	307.42	307.09 ± 0.24
		4.34 ± 1.1e-05		−1.42 ± 2.4e-05		152.41 ± 0.15		307.11 ± 0.24
K_1	1.94	1.72 ± 0.18	−0.95	−0.84 ± 0.09	135.40	135.57 ± 0.12	111.42	111.23 ± 0.13
		1.94 ± 9.9e-06		−0.95 ± 1.5e-05		135.62 ± 0.17		111.25 ± 0.13
O_1	1.37	1.21 ± 0.13	−0.68	−0.60 ± 0.07	133.24	133.39 ± 0.11	117.78	117.58 ± 0.14
		1.37 ± 6.7e-06		−0.68 ± 9.9e-06		133.44 ± 0.16		117.60 ± 0.14

than those of $\hat{\psi}_1$. While $\tilde{\psi}$ represents only 2% of the variance of ψ as a bulk measure over the water column, evaluating at $z = 3.5$ m above the bottom, $\tilde{\psi}$ accounts for 11% of the variance of ψ. This near-bottom variance in $\tilde{\psi}$ corresponds to an M_2 semimajor axis amplitude of 4.78 cm s^{-1}, which is statistically significant and would suggest the presence of an internal tide despite the purely barotropic formulation used to synthesize the time series.

The linear eddy viscosity model used to provide a realistic vertical profile is frequency dependent. The vertical scale of the bottom boundary layer depends on the difference between the tidal frequency and that of the local inertial frequency. To examine CEOF performance in recovering barotropic vertical structure of a signal containing multiple tidal frequencies (each with slightly different boundary layer scales), time series were synthesized with the five most significant tidal constituents on this part of the shelf (Blanton et al. 2004): M_2, N_2, S_2, K_1, and O_1. Near-surface synthetic semimajor axes specified by the synthetic signal are given in the first two columns of Table 1. The depth-average $\overline{\psi}_z$ underestimates the M_2 semimajor and semiminor axes by 3.98 and 1.58 cm s^{-1}, respectively, near surface; near-bottom overestimates (not shown) are 8.4 and 2.9 cm s^{-1}. Comparable to the single-frequency analysis, $\hat{\psi}_0$ contains 99.999% of the variance of the multiple frequency synthetic record. The bulk of the remainder of the variance lies in $\hat{\psi}_1$, and is not significant; confidence intervals about the $\hat{\psi}_1$-calculated semiaxes lengths are one–two orders of magnitude smaller than could be practically measured for typical ADCP configurations used to measure velocity over the water column on the shelf.

Using synthetic velocity data generated for a shallow water shelf, CEOF analysis recovers the known vertical structure of the barotropic tide at a single frequency into the lowest mode. The CEOF technique is a significant improvement over depth-averaging methods, which suggest the presence of baroclinic tidal motions in the synthetic signal where none were prescribed by the purely barotropic formulation. This successful estimation of a zero amplitude baroclinic current is repeatable with synthesis of multiple tidal frequencies with slightly varying vertical structures.

b. R_6 data

Having shown that CEOF analysis can represent in its gravest mode a frictionally modified barotropic tide comprising multiple frequencies with slightly varying but known vertical structure, the analysis is repeated for data measured by an ADCP over the same time period at the same location. The structure of any internal tide present in the measured data is not known a priori, but the generally well-mixed conditions under which the observations were collected suggest that baroclinic tidal motions cannot be supported. Thus, as in the previous section, $\tilde{\psi}$ and $\hat{\psi}_1$ are not expected to represent an internal tide but rather a measure of error of the estimates of the barotropic tide given by $\overline{\psi}_z(t)$ and $\hat{\psi}_0$, respectively, using depth-averaging and CEOF methods. Hourly unfiltered data are used as input.

The lowest CEOF mode $\hat{\psi}_0$ captures 99.36% of the variance over the month, with $\hat{\psi}_1$ and $\hat{\psi}_2$ containing 0.55% and 0.06%, respectively. The variance in $\hat{\psi}_2$ and higher modes is small enough that $\hat{\psi}_1$ can be interpreted as the EOF estimate of baroclinic current structure in ψ. Four-day time series of the u and v components of ψ at $z = 3.5$ mab (Fig. 4) suggest M_2 tidal currents on the order of 25–30 cm s^{-1} occur near bottom. Time series of the tidal fits to the estimates of baroclinic currents formed by depth-averaging and CEOF methods, $\tilde{\psi}$ and $\hat{\psi}_1$ differ by an order of magnitude. Near-bottom $\tilde{\psi}$ is directed opposite the near-bottom measured velocity,

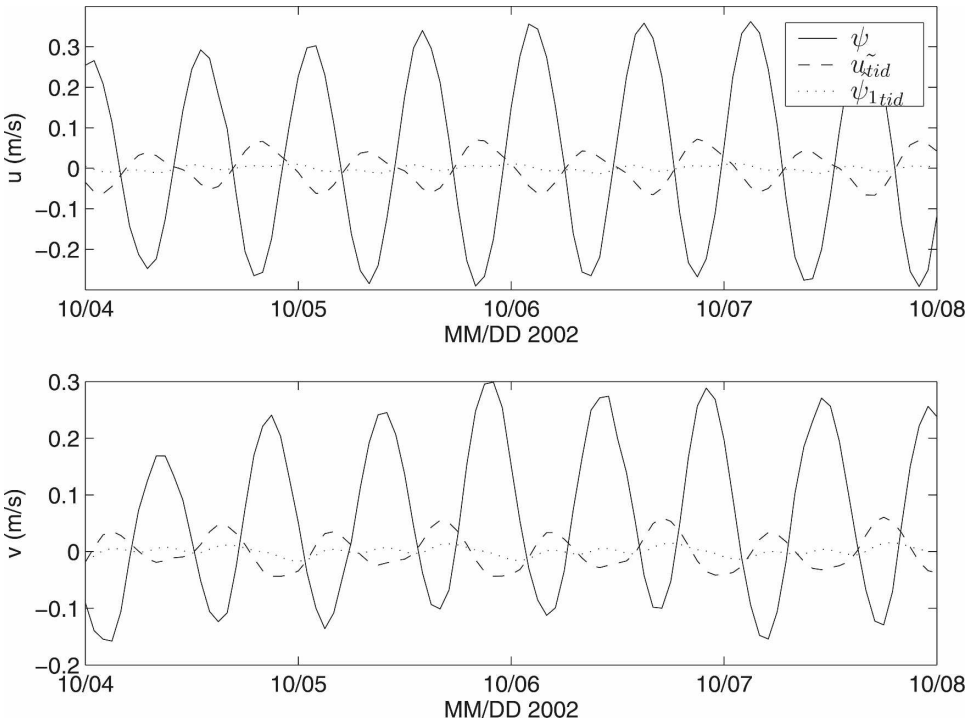

FIG. 4. Time series of the u and v components of $\psi(z, t)$ (solid line) and the tidal fits to $\tilde{\psi}(z, t)$ (dashed line) and $\hat{\psi}_1(z, t)$ (dotted line) at $z = 3.5$ m above the bottom over a 4-day period in October 2002.

and is largely anticorrelated with ψ. Variability of $\hat{\psi}_1$ is less tidal than that of $\tilde{\psi}$; the 29 tidal constituents resolved in a 30-day time series account for approximately 30% of the variance in $\hat{\psi}_1$ and 70% of the variance of $\tilde{\psi}$.

The M_2 tidal ellipses of ψ (Fig. 5a) are oriented cross-shore and are reproduced to within 2 cm s^{-1} by the $\hat{\psi}_0$ ellipses (Fig. 5b). Confidence intervals about $\hat{\psi}_0$ represent between 2.4% and 4.1% of the semiaxes lengths and are less than 4° for orientation and phase. Tidal ellipses of the $\tilde{\psi}$ (Fig. 5c) have a trend in the vertical similar to that of the synthetic data—the near-bottom semiaxes reflect the presence of the frictional boundary layer, with about twice the magnitude of near-surface values (4.18 versus 2.12 cm s^{-1} semimajor axis speeds, respectively). The $\tilde{\psi}$ ellipses (Fig. 5c) near surface lie within 10° of the orientation of the full-signal ellipses, with a 180° phase difference surface to bottom. The phases of ψ vary less than a degree over the water column, but $\tilde{\psi}$ M_2 phase changes about 10° over the deepest 5 m.

In contrast, the $\hat{\psi}_1$ M_2 ellipses (Fig. 5d) are nearly rectilinear, with the semimajor axis 20° counterclockwise of the orientation of that of ψ and the largest values near surface (max $u_{\text{major}} = 1.18$ cm s^{-1}, max $u_{\text{minor}} = 0.014$ cm s^{-1}). In the mean, $\hat{\psi}_1$ semimajor and semiminor axes are approximately one and two orders of magnitude smaller than those of the values for $\tilde{\psi}$. The 95% confidence intervals indicate $\hat{\psi}_1$ to be not significantly different from zero. The lack of energy in higher empirical modes suggests that M_2 internal tidal motions are not present in the data, which conflicts with the prediction using depth-averaging methods that baroclinic M_2 tidal currents in the measured data are on the order of several centimeters per second.

A comparison of $\tilde{\psi}$ given synthetic and measured time series as input currents supports the hypothesis that bottom boundary layer dynamics are responsible for the energy in $\tilde{\psi}$. The shape and magnitude of the profiles of M_2 semimajor and semiminor axes of $\tilde{\psi}$ given synthetic and measured time series are compared (Fig. 6). The similarity in shape and size of the profiles of M_2 ellipse parameters calculated for measured data and a purely barotropic formulation substantiates the assumption that the relatively well-mixed water column should not be able to support baroclinic tidal motion. Since friction (modified by rotation) is the only source of shear in the Soulsby (1990) formulation of the synthetic ψ, this resemblance of $\tilde{\psi}$ for measured data to $\tilde{\psi}$ for a purely barotropic synthetic profile indicates that the variance in $\tilde{\psi}$ of measured current data is likely due to bottom boundary effects.

The diurnal tides are significantly less energetic than the semidiurnal tides on the SAB (Table 1), but the

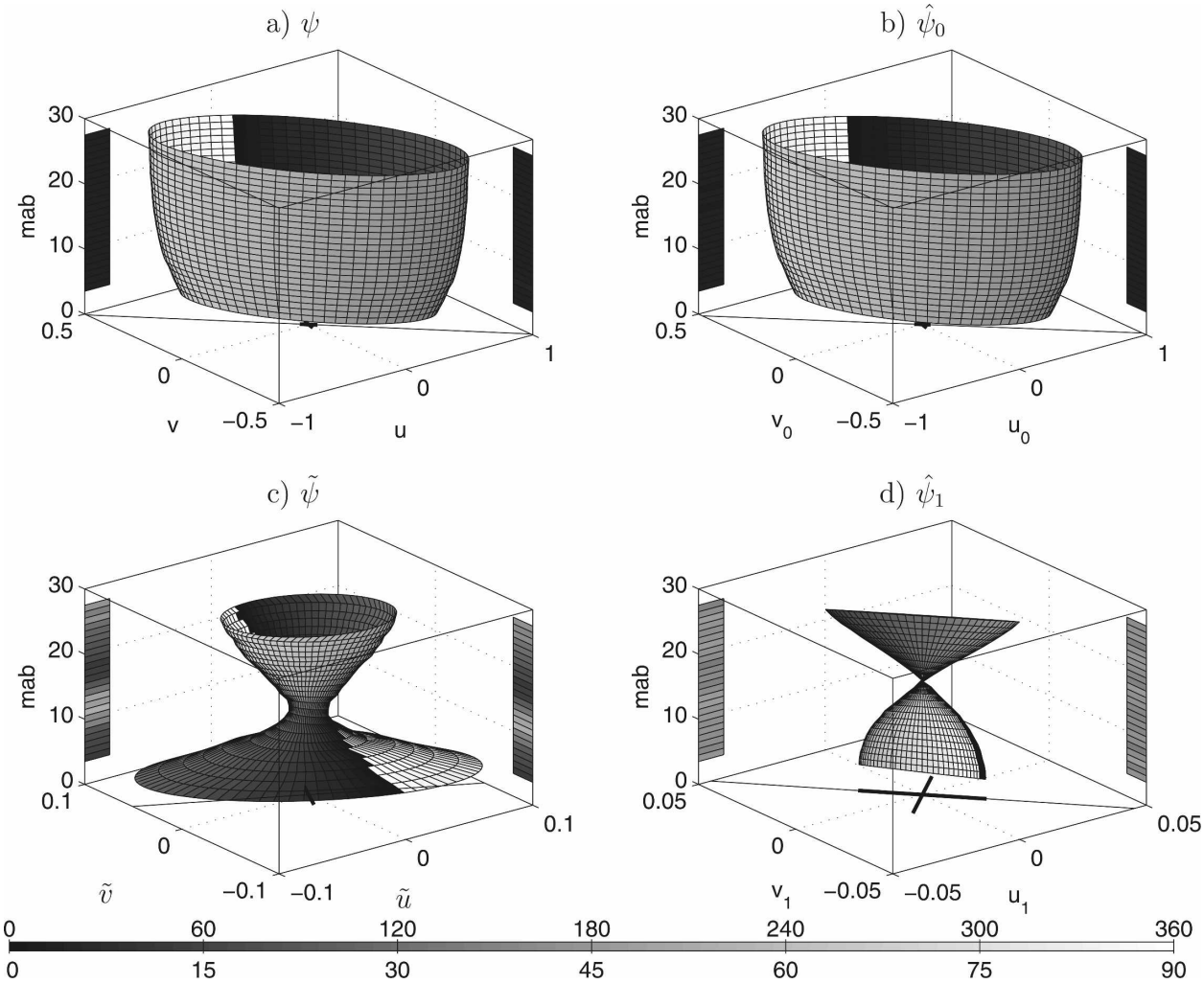

FIG. 5. The M_2 tidal ellipses and ellipse parameter errors for October 2002 data: (a) the original signal $\psi(z, t)$, (b) $\hat{\psi}_0(z, t)$, (c) $\tilde{\psi}(z, t)$, and (d) $\hat{\psi}_1(z, t)$, following the same convention as in Fig. 3. Ellipse semiaxes and semiaxis errors are normalized by the semimajor axis of the near-surface ellipse of the synthetic signal shown in Fig. 3a. Note the difference in scale from Fig. 3.

height of the bottom boundary layer associated with a tidal current is inversely proportional to the difference between the local inertial frequency f and tidal frequency (Soulsby 1990). At this latitude, K_1 and O_1 lie at frequencies that approach the singularity at the inertial frequency (0.96f and 0.89f, respectively), and the effects of bottom friction on the diurnal tide can theoretically reach to nearly the height of the water column. The K_1 tidal ellipses of ψ (Fig. 7a) are larger in magnitude than predicted by the tidal database of Blanton et al. (2004). However, the magnitude and shape of $\hat{\psi}_0$ in the vertical are in closer agreement to the expected vertical profile of the diurnal tide at this latitude. Further, in comparison to ψ, the tidal fit to $\hat{\psi}_0$ is significantly improved, with smaller confidence intervals about the semiaxes, inclination, and phase (Fig. 7b). The K_1 tidal fit to $\tilde{\psi}$ is not smooth in either the vertical or phase (Fig. 7c), and 95% confidence intervals about the ellipse magnitudes indicate that the fits to the $\tilde{\psi}$ and $\hat{\psi}_1$ are not significant. Confidence intervals about the $\hat{\psi}_1$ ellipse phase are smaller than those for the $\tilde{\psi}$, but errors in orientation are larger because of the more circular shape.

Analysis of the O_1 constituent present in ψ (Fig. 8a) yields a pronounced increase in signal strength relative to Blanton et al. (2004), but with a distinct conical shape to the tidal ellipses with depth. Confidence intervals about ellipse orientation and phase for all O_1 tidal ellipses are large because of the ambiguity in orientation of a nearly circular ellipse. Tidal analysis of $\hat{\psi}_0$ recovers a signal that more closely resembles a frictional boundary layer associated with the barotropic tide (Fig. 8b). Near bottom, the magnitude of O_1 is

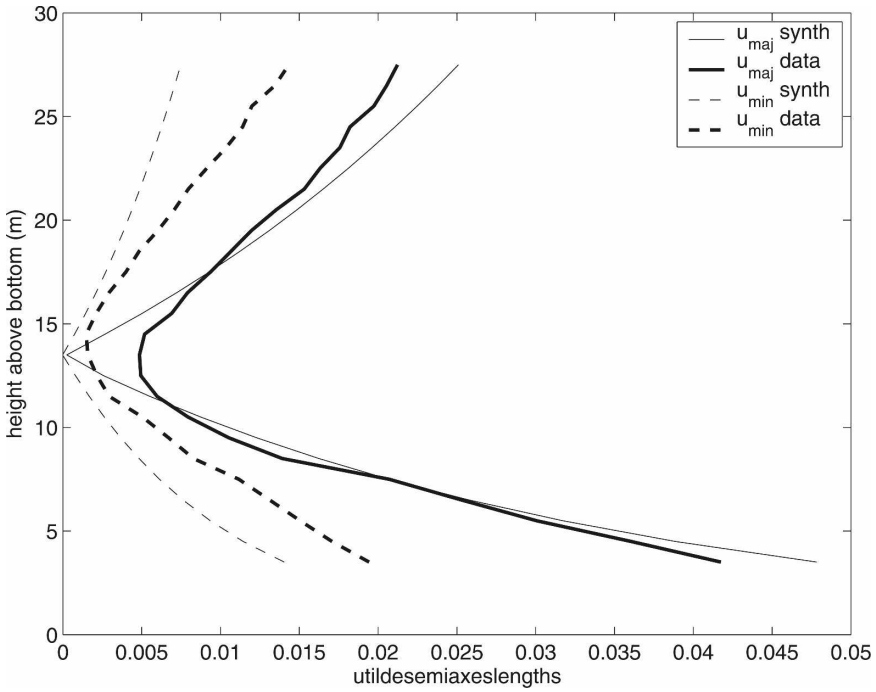

FIG. 6. Profiles of M_2 ellipse semiaxis lengths calculated for synthetic (thin lines) and measured (thick lines) representations of $\tilde{\psi}(z, t)$. The solid and dashed lines indicate the semimajor and semiminor axes u_{maj} and u_{min} (m s^{-1}).

greater than the tidal analysis of the ψ indicates. However, the difference between the profiles of the $\hat{\psi}_0$ and ψ ellipses suggests a superposition of internal and external modes at this frequency. Both the $\tilde{\psi}$ and $\hat{\psi}_1$ ellipses are of statistically significant magnitudes (on the order of 1–2 cm s^{-1}) and have similar profile shape in the vertical (Figs. 8c,d), but near surface, $\hat{\psi}_1$ is more consistent.

Summarizing this section, CEOF analysis yields an estimate of barotropic tidal currents that includes the frictional boundary layer structure primarily associated with barotropic tidal dynamics; depth-averaging methods assume that any vertical variability in the measured velocity time series is due to baroclinic motion. Tidal analysis of $\tilde{\psi}$ suggests significant internal tidal currents at the M_2 and O_1 frequencies, whereas analysis of $\hat{\psi}_1$ indicated significant internal tidal variability only at the O_1 frequency. The estimates of barotropic tidal motion using depth-averaging and EOF methods produce conflicting predictions of the frequencies at which there is meaningful baroclinic variability.

4. Discussion

In both idealized shallow water records of tidal currents and field-measured currents, CEOF analysis provides a better estimate of the barotropic tide than depth-averaging methods and thus can allow a more accurate representation of internal tides in measured data in shallow water. The representation of the barotropic tide as a depth-averaged signal cannot account for the modification of the barotropic tide by bottom friction. When the internal tidal structure is estimated by subtracting the depth average from the original signal, frictional effects can be misinterpreted as arising from the baroclinic tide, for example, the M_2 signal in $\tilde{\psi}$ for both the synthetic and measured datasets. Estimates of barotropic tidal currents using CEOF analysis can retain in $\hat{\psi}_0$ this frictional boundary layer as part of the barotropic tide, providing a more accurate representation of internal structure in higher modes.

Though the data and time frame used here for comparison of CEOF and depth-averaging methods was primarily chosen to minimize potential internal tidal variability, both methods of separating the surface and internal tides identify an unanticipated internal structure given the well-mixed conditions. At this latitude (31.4°N), diurnal tidal frequencies fall into the inertial/near-inertial band, and the tidal and near-inertial processes can be harmonically indistinguishable given a time series of this length. While the strength and vertical structure of $\hat{\psi}_0$ at O_1 and K_1 are consistent with that

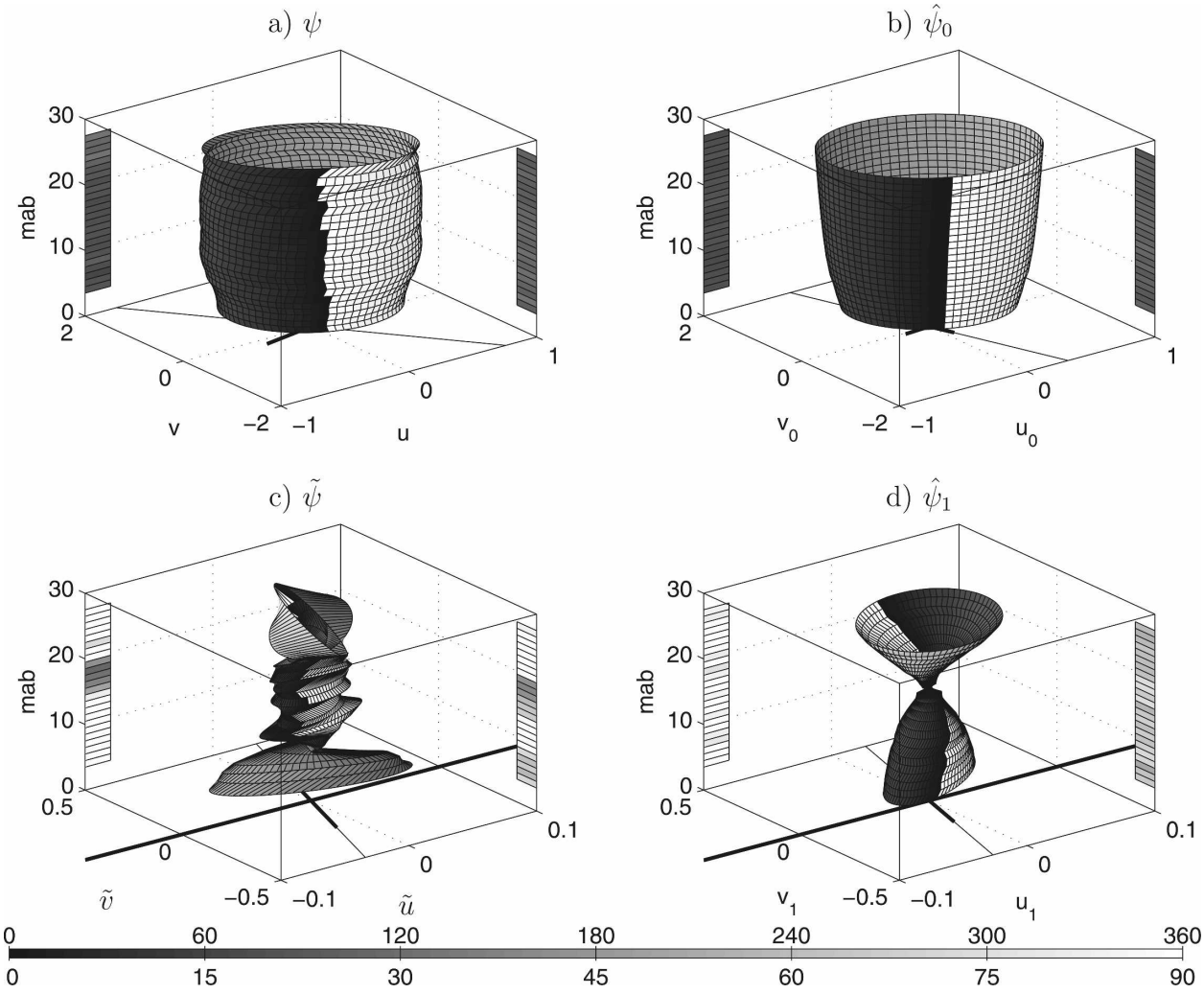

FIG. 7. The K_1 tidal ellipses and ellipse parameter errors for October 2002 data: (a) the original signal $\psi(z, t)$, (b) $\hat{\psi}_0(z, t)$, (c) $\tilde{\psi}(z, t)$, and (d) $\hat{\psi}_1(z, t)$, following the same convention as Fig. 3. Ellipse semiaxes and semiaxis errors are normalized by the semimajor axis of the near-surface ellipse of the synthetic K_1 signal shown in Table 1.

of barotropic tidal currents, the signal in $\hat{\psi}_1$ suggests an inertial response. The mode 1 shape of the diurnal/near-diurnal variability may be attributed to inertial oscillations near a coastal boundary rather than the baroclinicity of the mass field (Rippeth et al. 2002; Davies and Xing 2003). CEOF analysis separates the signal into modes that allow interpretation of the diurnal band as dominated by a tidal signal apparent in $\hat{\psi}_0$ and wind-forced inertial/near-inertial oscillations apparent in $\hat{\psi}_1$. While the variance in $\hat{\psi}_1$ is less than 1% of the total variance, the signal represents currents of 2–3 cm s^{-1}, approaching or exceeding the magnitude of $\hat{\psi}_0$ in the diurnal band. The unpredicted energy in $\hat{\psi}_1$ in the diurnal band indicates that the CEOF method correctly separates into independent modes two processes that are indistinguishable via harmonic analysis. Potential forcing by diurnal sea breeze and near-resonant response is beyond the scope of this analysis but is currently being explored.

Both CEOF and depth-averaging methods agree in predicting significant energy at O_1 that is not explained by the barotropic tide, and an inertial response is a plausible physical mechanism to explain the presence of increased diurnal energy at this latitude. However, separating the barotropic and baroclinic tidal currents using depth-averaging methods suggests an energetic M_2 internal tide of 2–5 cm s^{-1}, which is not predicted by CEOF analysis. The resemblance of $\tilde{\psi}$ for measured data to the synthetic barotropic signal supports the notion that bottom boundary layer structure associated with the barotropic tidal dynamics can mistakenly be interpreted to result from an internal tide when depth

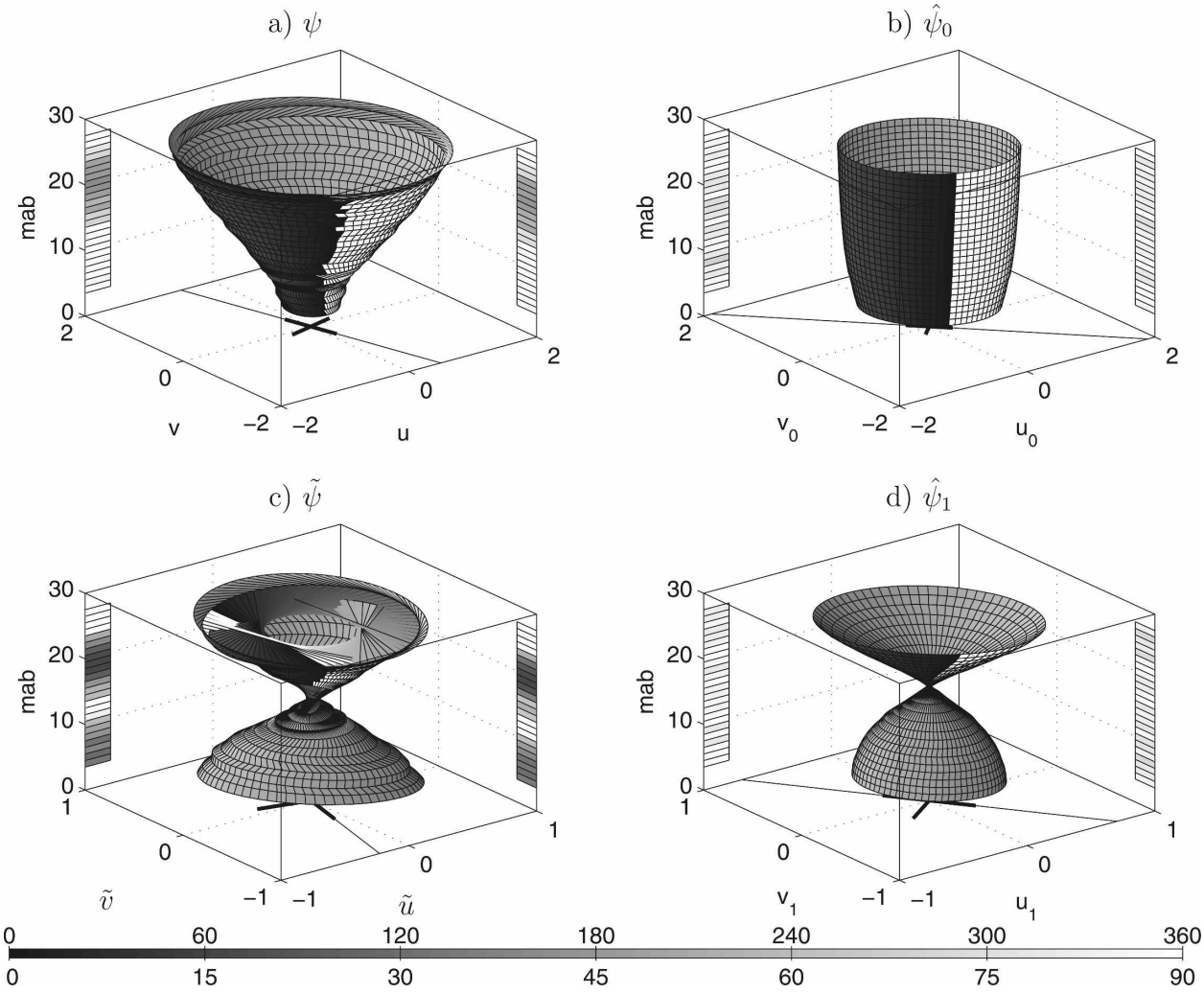

FIG. 8. The O_1 tidal ellipses and ellipse parameter errors for October 2002 data: (a) the original signal $\psi(z, t)$, (b) $\hat{\psi}_0(z, t)$, (c) $\tilde{\psi}(z, t)$, and (d) $\hat{\psi}_1(z, t)$, following the same convention as Fig. 3. Ellipse semiaxes and semiaxis errors are normalized by the semimajor axis of the near-surface ellipse of the synthetic O_1 signal shown in Table 1.

averaging is employed in shallow water. The present results suggest that CEOF analysis allows for a better representation of the vertical structure of internal waves and tides in energetic shallow water environments.

As with any empirical method, however, careful consideration must be given to the applicability of the method and particularly to interpretation of the results. The analysis above interprets the lowest CEOF mode to be the barotropic tidal motion modified by bottom friction, with the higher orthogonal modes indicating energy in the baroclinic tide. While the empirical modes are by definition orthogonal to each other and the input velocity can be represented by the linear sum of the modes, barotropic and baroclinic dynamics are not linearly independent. When nonlinear friction is important over much of the water column, there can be significant coupling of the barotropic and baroclinic tidal signals. The structure of the bottom boundary layer is set by the sum of barotropic and baroclinic velocities, but the analysis assumes each will be independently modified by friction. In this coupling of barotropic and baroclinic tidal dynamics by nonlinear friction, a challenge can arise in separating barotropic and baroclinic modes when the amplitudes of the modes are comparable and thus both contribute significantly to the frictional response. Semidiurnal internal tidal currents in the SAB are not expected to be comparable to the 30–40 cm s^{-1} barotropic tidal current signal, but the analysis above predicts $\hat{\psi}_1$ to be of the same order as $\hat{\psi}_0$ at the O_1 frequency. Here, the two signals at O_1 have been interpreted as arising from nontidal and tidal dy-

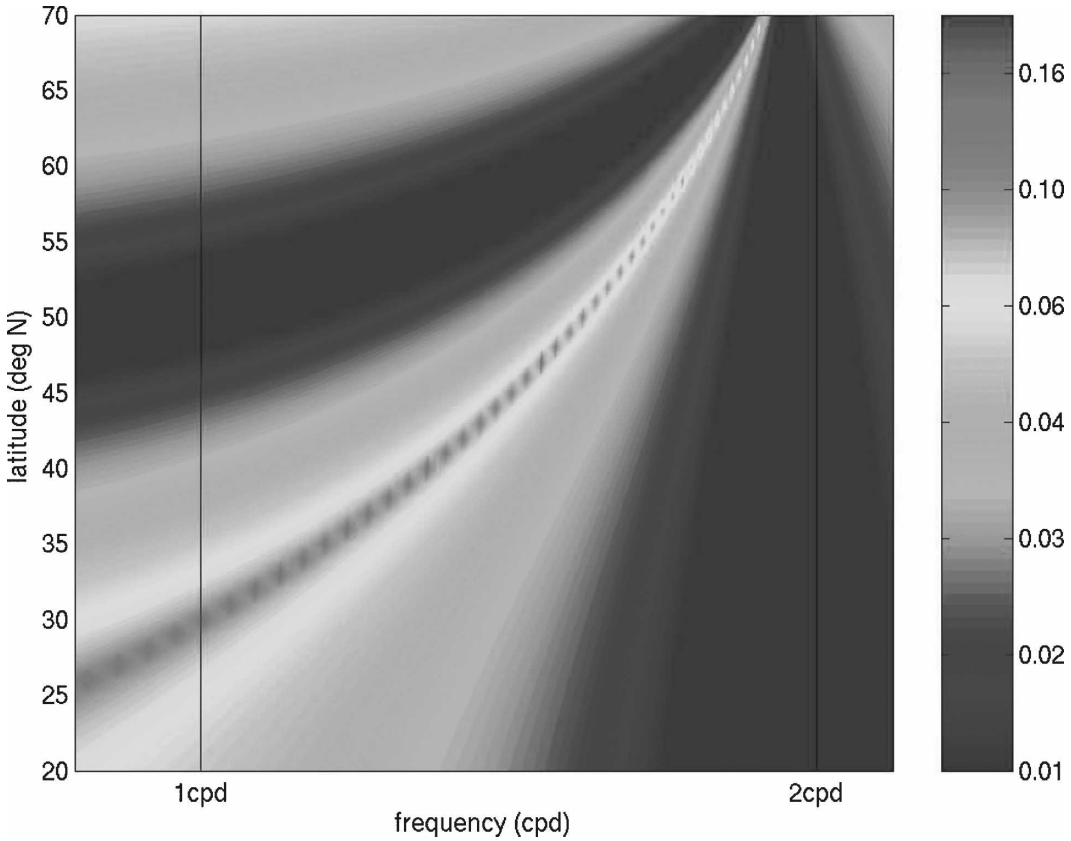

FIG. 9. Normalized bulk error in assuming the vertical structure of M_2 for tidal currents of a given frequency over a range of latitudes. The error estimate is formed by vertically averaging the magnitude of the vector difference between normalized tidal current profiles relative to M_2 using the linear eddy viscosity model of Soulsby (1990).

namics and the total energy in the higher modes is much less than that of $\hat{\psi}_0$, but the degree to which the coupling of barotropic and baroclinic modes hampers their separation using CEOF analysis remains unclear.

The CEOF method allows for the analysis of inertial oscillations or internal tidal motions that may or may not be phase or frequency locked to barotropic processes. In contrast, removing a depth average of a tidal current imposes direction and phase information on the resultant estimate of baroclinic currents. Near surface, $\overline{\psi}$ underestimates the barotropic flow by several centimeters per second in the SAB, which results in a near-surface $\tilde{\psi}$ that is in phase with $\overline{\psi}(t)$. Near bottom, where the overestimate of the barotropic currents can be tens of centimeters per second, depth averaging casts a 180° phase difference between $\overline{\psi}(t)$ and near-bottom $\tilde{\psi}$.

The CEOF method's assumption of independence of vertical and temporal variability can break down when vertical structure is dependent on time or frequency content. Analysis of synthetic tidal data containing multiple tidal frequencies successfully recovered these slightly varying vertical structures into the lowest mode. Application of the method to several years' worth of ADCP currents measured on the SAB in water depths ranging from 15 to 45 m (not shown) yields similar results as those presented here for a midshelf location—the boundary layer structure of barotropic currents is contained in the lowest mode, allowing for a more accurate estimate of the internal structure. However, practical experience with multiyear time series over this spatial array suggests particular consideration be paid to the time scales over which the character of the profiles may change. In the SAB, seasonal stratification appears to be the most important control. Time series lengths greater than 3 months tend to yield a decomposition in which the gravest mode can no longer fully describe the barotropic tide, and part of the variance is shunted to a higher mode. This result is consistent with observational estimates of bottom boundary layer thickness that suggest that the height of the bottom boundary layer changes as the seasonal stratification varies (M. Muglia 2004, personal communication). Experimentation with input time series length can be a useful indicator of validity of the assumption

that the lowest mode fully contains the barotropic tide. Significant change in structure advises shorter input time series length, with a minimum given by the Rayleigh criterion for the frequency resolution of interest.

An estimate of the error in neglecting slight differences in vertical structures among the dominant semidiurnal M_2 and the other major constituents can be calculated using Soulsby's (1990) linear eddy viscosity model over a range of tidal frequencies and latitudes. The depth-averaged normalized difference between the vertical structure of M_2 and tidal frequencies between 0.75 and 2.25 cpd is examined (Fig. 9), assuming that the frequencies compared have the same magnitude of free-stream velocity maximum. Errors are greatest at the local inertial frequency, where the singularity in the Soulsby (1990) formulation gives a boundary layer of infinite vertical extent. Increasing the northern latitudinal bound of Fig. 9 would reveal a second error maximum at the latitude where the M_2 tide becomes critical (74.48°N). For this application, the depth-averaged normalized error is as large as 11% for K_1, but the CEOF approach is able to aggregate all synthetic tidal frequencies into a single mode (Table 1), which suggests some degree of flexibility in application of the method, even at a latitude where expected error is large.

5. Summary

A CEOF method of separating the barotropic and baroclinic tidal velocity structures is shown to be a significant improvement over assigning the depth-averaged current to be the barotropic component in shallow water. The representation of baroclinic tidal motions as the difference between velocity profiles and a depth average cannot account for frictional shear in the bottom boundary layer and results in an overestimate of internal tidal motions that can resemble a bottom-trapped internal tide. CEOF analysis reduces the error in removing a synthetic barotropic signal modified by friction. Application of the method to measured data suggests similar advantages over depth averaging. Whereas the analysis of $\tilde{\psi}$ suggests multiple possible internal modes of motion at tidal frequencies, the EOF method unambiguously separates a potentially wind-forced structure (i.e., near-inertial motion) from the barotropic tide despite the overlay in frequency space. The successful application of the method to unfiltered data measured in an energetic shallow water environment of the SAB constitutes a significant test of the method, and suggests that CEOF analysis can be a valuable tool for the investigation of internal waves, inertial motions, and tides on continental shelves and in other shallow water environments.

Acknowledgments. The authors thank John M. Bane, Francisco E. Werner, and Alberto D. Scotti for their suggestions in preparation of the manuscript, as well as two anonymous reviewers for their comments. This analysis was supported as part of SEACOOS, sponsored by the Office of Naval Research under Award N00014-02-1-0972. C. Edwards has also been supported by the Royster Society of Fellows.

REFERENCES

Apel, J. R., and Coauthors, 1997: An overview of the 1995 SWARM shallow-water internal wave acoustic scattering experiment. *IEEE J. Oceanic Eng.,* **22,** 465–500.

Barnett, T. P., 1985: Variations in near-global sea level pressure. *J. Atmos. Sci.,* **42,** 478–501.

Blanton, B., and Coauthors, 2004: Barotropic tides in the South Atlantic Bight. *J. Geophys. Res.,* **109,** C12024, doi:10.1029/2004JC002455.

Davies, A. M., and J. Xing, 2003: Processes influencing wind-induced current profiles in near coastal stratified regions. *Cont. Shelf Res.,* **23,** 1379–1400.

Davis, R. E., 1976: Predictability of sea surface temperature and sea level pressure anomalies over the North Pacific Ocean. *J. Phys. Oceanogr.,* **6,** 249–266.

Hall, P., and A. M. Davies, 2002: Analysis of time-varying wind-induced currents in the North Channel of the Irish Sea, using empirical orthogonal functions and harmonic decomposition. *Cont. Shelf Res.,* **22,** 1269–1300.

Holloway, P. E., P. G. Chatwin, and P. Craig, 2001: Internal tide observations from the Australian North West Shelf in summer 1995. *J. Phys. Oceanogr.,* **31,** 1182–1199.

Horel, J. D., 1984: Complex principal component analysis: Theory and examples. *J. Climate Appl. Meteor.,* **23,** 1660–1673.

Huthnance, J. M., 1989: Internal tides and waves near the continental shelf edge. *Geophys. Astrophys. Fluid Dyn.,* **48,** 81–106.

Kaihatu, J. M., R. A. Handler, G. O. Marmorino, and L. K. Shay, 1998: Empirical orthogonal function analysis of ocean surface currents using complex and real-vector methods. *J. Atmos. Oceanic Technol.,* **15,** 397–414.

Lee, T. N., and D. A. Brooks, 1979: Initial observations of current, temperature, and coastal sea level response to atmospheric and Gulf Stream forcing on the Georgia shelf. *Geophys. Res. Lett.,* **6,** 321–324.

——, J. A. Yoder, and L. P. Atkinson, 1991: Gulf Stream frontal eddy influence on productivity of the Southeast U.S. continental shelf. *J. Geophys. Res.,* **92,** 22 191–22 205.

Lentz, S. J., 1994: Current dynamics over the northern California inner shelf. *J. Phys. Oceanogr.,* **24,** 2461–2478.

Lerczak, J. A., C. D. Winant, and M. C. Hendershott, 2003: Observations of the semidiurnal internal tide on the southern California slope and shelf. *J. Geophys. Res.,* **108,** 3068, doi:10.1029/2001JC001128.

MacKinnon, J. A., and M. C. Gregg, 2003a: Shear and baroclinic energy flux on the summer New England shelf. *J. Phys. Oceanogr.,* **33,** 1462–1475.

——, and ——, 2003b: Mixing on the late-summer New England shelf—Solibores, shear, and stratification. *J. Phys. Oceanogr.,* **33,** 1476–1492.

Münchow, A., and R. J. Chant, 2000: Kinematics of inner shelf

motions during the summer stratified season off New Jersey. *J. Phys. Oceanogr.,* **30,** 247–268.

Pawlowicz, R., B. Beardsley, and S. Lentz, 2002: Classical tidal harmonic analysis including error estimates in MATLAB using T_TIDE. *Comput. Geosci.,* **28,** 929–937.

Preisendorfer, R. W., 1988: *Principal Component Analysis in Meteorology and Oceanography.* Elsevier, 426 pp.

Redfield, A. C., 1958: The influence of the continental shelf on the tides of the Atlantic coast of the United States. *J. Mar. Res.,* **17,** 432–448.

Rippeth, T. P., and M. E. Inall, 2002: Observations of the internal tide and associated mixing across the Malin Shelf. *J. Geophys. Res.,* **107,** 3028, doi:10.1029/2000JC000761.

——, J. H. Simpson, R. J. Player, and M. Garcia, 2002: Current oscillations in the diurnal-inertial band on the Catalonian shelf in spring. *Cont. Shelf Res.,* **22,** 247–265.

Seim, H. E., 2000: Implementation of the South Atlantic Bight Synoptic Offshore Observational Network. *Oceanography,* **13,** 18–23.

Simionato, C. G., V. Meccia, W. Dragani, and M. Nuñez, 2005: Barotropic tide and baroclinic waves observations in the Río de la Plata estuary. *J. Geophys. Res.,* **110,** C06008, doi:10.1029/2004JC002842.

Soulsby, R. L., 1990: Tidal-current boundary layers. *The Sea,* B. L. Mehaute and D. Hanes, Eds., Vol. 9, *Ocean Engineering Science,* Wiley, 523–566.

Tebeau, P. A., and T. N. Lee, 1979: Wind induced circulation on the Georgia shelf. University of Miami Tech. Rep. 79003, 177 pp.

Weber, A. H., and J. O. Blanton, 1980: Monthly mean wind fields for the South Atlantic Bight. *J. Phys. Oceanogr.,* **10,** 1256–1263.

Webster, I., 1986: The vertical structure of currents on the North West Shelf of Australia at subtidal frequencies. *J. Phys. Oceanogr.,* **16,** 1145–1157.